CBPF-NF-044/81

CHARGE OSCILLATIONS IN ORBITRONS

by

M.Porto* and L.C.Gomes

*DEPARTAMENTO DE FÍSICA NUCLEAR
INSTITUTO DE FISICA DA UNIVERSIDADE DE SÃO PAULO
CAIXA POSTAL 20516
01500 - São Paulo - SP - BRASIL

CENTRO BRASILEIRO DE PESQUISAS FÍSICAS - CBPF/CNPq
Av. Wenceslau Braz, 71, fundos
22290 - Rio de Janeiro - RJ - BRASIL

ABSTRACT

A statistical model for the electron distribution in orbitrons is constructed where the effect of the end plates is considered. A comparison is made with the measured density of charge. The electromagnetic oscillations generated by orbitrons are calculated as pressure waves and the results obtained are compared with the data.

RESUMO

É construído um modelo estatístico para a distribuição de elétrons dentro do órbitron que leva em conta o comprimento finito do aparelho. É feita uma comparação com a distribuição de carga medida experimentalmente. As oscilações eletromagnéticas geradas pelo órbitron são calculadas como ondas de pressão e os resultados obtidos são comparados com os dados experimentais.

1. INTRODUCTION

In a previous paper (1) we have analysed the charge distribution in orbitrons and compared our results to the experimental data obtained by Cybulska and Douglas (2). Our basic hypothesis was that the electrons would always estabilish a local thermal equilibrium in the observed steady state of the charge distribution. The filament injects electrons very far from this equilibrium situation and our hipothesis is equivalent to say that the relaxation time for the initial distribution injected by the filament to reach the steady state distribution described by our model is shorter than the mean life time of the electron in the orbitron. The opposite assumption is behind the considerations of Hooverman (3), Feaks et al. (4) and Deichelbohrer (5).

These authors assumed that the electron distribution is determined by the individual unperturbed orbits of the electrons that come from the filament region. Therefore the local statistical equilibrium assumed by us is suposed never to be reached and equivalently the relaxation time refered to above is suposed to be much longer than the mean life time of the electron inside the orbitron. Calculations of relaxation times are a difficult task and we have relied on the agreement of our model to the experimental data of Cybulska and Douglas (2) to set out this controversial point. Extensive analysis of Porto Pato (6) based on the assumption of independent trajectories of the electrons from the filament region have shown to be unable to explain the experimental data of Cybulska and Douglas (2).

The situation with the statistical model for the electron distribution is different. We have obtained a reasonably good agreement with the experimental data, with a single adjustable parameter (the equilibrium temperature of the electrons in the steady state).

In this paper we will improve our previous calculations by considering partially the effect of the end plates on the distribution. We then calculate the eletromagnetic oscillations generated by the orbitron as pressure waves in the electron distribution and compared with the experimental results of Troise et al. (7).

2. THE ELECTRON DENSITY FUNCTION

As we have argued in reference (1), the steady state phase space distribution function for the electrons inside the orbitron is given by

$$f(r,\rho) = A \exp\left[-H(p,r)/kT\right] \qquad p \in D \qquad (2.1)$$

subjected to the constraint that p should be inside a the domain D caracterized by the orbits that do not touch the boundaries of the orbitron. For p outside D f is zero. In eq. (2.1) H(p,r) is the single particle hamiltonian for the electron:

$$H(p,r) = \frac{p^2}{2m} + e\,V(r) \quad , \qquad (2.2)$$

k is the Boltzmann constant, T the temperature of the electrons in the steady state and A a normalization constant. The potential V(r) can be considered as the mean electrostatic potential in which one takes into account self consistently the effect of the space charge of the electrons. For the applications we have in mind, we will neglect the space charge effect and set

$$V(r) = V_a \frac{\log(r/b)}{\log(a/b)}$$

where V_a is the anode electrostatic potential and a and b are the anode and cathode radii respectively.

The spatial distribution is given by

$$n(r) = \int_D f(\vec{r},\vec{p})\, d^3p \quad , \tag{2.3}$$

and the essential point in our model for $n(r)$ is the specification of the domain D. This domain is specified by the kinematical considerations that follows. It is well recognised that the electrons in orbitrons, have a very long mean free path. We assume that once the trajectory of the electron is such as to be able to make contact with its metal environment, the electron is absorbed. We therefore fix the domain D by excluding from $f(r,p)$ every momenta p that lead to trajectories that touch the anode or the cathode. To prevent the electrons from touching the cathode its enough to assume that their energies are negative. Using cylindrical coordinates we have

$$\frac{p_r^2}{2m} + \frac{L^2}{2mr^2} + \frac{p_z^2}{2m} - e\,V(r) < 0 \quad . \tag{2.4}$$

The electrons that do not collide with the anode are those that the angular momentum L is larger than a minimum value fixed by the radius a of the anode

$$L > L_{im} = a\sqrt{2m(H - \frac{p_z^2}{2m} + c\,V_a)} \tag{2.5}$$

Let us introduce dimensionless quantities defining the variables:

$$x = r/b \quad ,$$

$$u = p_r/(2m\sqrt{kT}) \quad ,$$

$$v = L/(2mr\sqrt{kT}) \quad ,$$

$$t = p_z/(2m\sqrt{kT})$$

and the constants

$$x_0 = a/b \tag{2.6}$$

and

$$\alpha = e\,V_a/(kT) \quad . \tag{2.7}$$

With these definitions eqs. (2.4) and (2.5) take the form

$$u^2 + v^2 + t^2 < \alpha F(x) \tag{2.8}$$

and

$$\left(\frac{x^2}{x_0^2} - 1\right) v^2 - u^2 > \alpha\left[1-F(x)\right] \tag{2.9}$$

where we introduced

$$F(x) = \log x/\log x_0 \quad .$$

One observes that the integration in eq. (2.3) transforms into integration over the (u,v,t)-space of the transformed domain D. It is in this space that D takes its simple geometrical meaning. Eq. (2.8) shows that D is inside of a sphere of radius $\alpha F(x)$ and eq. (2.9) shows that the other boundary of D is a hiperbolic cylinder with geratrix parallel to the t-axis.

Fig. 1 shows the traces of these two surfaces in the plane t=0. Defining v_1, v_2 and v_3 as in this figure, we have:

$$v_1 = \left[\alpha\left(1-F(x) \;/\; \left(x^2-x_0^2\right) \;/\; x_0^2\right)\right]^{1/2} , \qquad (2.10)$$

$$v_2 = x_0 \sqrt{\alpha}/x \qquad (2.11)$$

and

$$v_3 = \sqrt{\alpha F(x)} \quad . \qquad (2.12)$$

The density distribution may now be written as

$$n(x) = \text{const.} x\, e^{\alpha F(x)} \left[\int_{v_1}^{v_2} dv\, e^{-v^2} \int_0^{u_1(v)} du\, e^{-u^2} \int_0^{t_1(u,v)} dt\, e^{-t^2} + \int_{v_2}^{v_3} dv\, e^{-v^2} \int_0^{u_2(v)} du\, e^{-u^2} \int_0^{t_1(u,v)} dt\, e^{-t^2} \right] \qquad (2.13)$$

where

$$t_1(u,v) = \sqrt{\alpha F(x)-u^2-v^2}$$

$$u_1(v) = \left[(x^2-x_0^2)v^2/x_0^2-\alpha(1-F(x))\right]^{1/2} \qquad (2.14)$$

$$u_2(v) = \left[\alpha F(x)-v^2\right]^{1/2} \quad .$$

The constant of normalization in eq. (2.13) is fixed by

$$\int_{x_0}^{1} n(x)\,dx = 1 \quad .$$

We observe from eq. (2.13) that n(x) depends on two parameters: x_0, which is fixed once the geometry of the orbitron is given, and α, which is related to the steady state temperature of the electron cloud and has to be adjusted to the experimental data.

Fig. 2 exhibits n(x) plotted for different values of α. One observes that the larger the value of α more sharp is the maximum of the distribution near the anode and smaller is the value of x at the maximum. This can be easily understood as α is inversely proportional to T. (See eq. (2.5).) The larger the value of α smaller is the value of T and electrons with less kinetic energies are more strongly pushed towards the anode. The value of x_0 taken for the curves exhibited in Fig. 1 where those reported in (2). In Fig. 3 we exhibit the effect of varying x_0. By increasing x_0 the peak of the distribution shifts away from the anode. This is due to the fact the only electrons with larger angular momenta are allowed in the distribution. This effect is very important for the understanding of the orbitron as an ion pump. The titanium cylinder (8) is what determines the radius of the anode and being appreciably large it shifts the peak of the distribution away from the anode having the effect of increasing the effective volume of the orbitron.

The density of electrons as a function of the radial distance r to the anode was indirectly observed by Cybulska and Douglas (2) by measuring the energy spectrum dI/dE of positive ions collected at the cathode in the limit of zero pressure. This spectrum can be connected to the ion current ($dI/d\Omega$) produced by unit of volume in the electron cloud as

$$\frac{dI}{dE} = \frac{dI}{d\Omega}\frac{d\Omega}{dE} = \frac{2\pi r}{e}\left(\frac{dV}{dr}\right)^{-1}\frac{dI}{d\Omega} \quad .$$

On the other hand $dI/d\Omega$ is given by

$$\frac{dI}{d\Omega} = c\, Nr_0 \int d^3p\, v\sigma\, (p^2/2m) f(r,p) \quad ,$$

where N is the total number of electron per unit of length in the orbitron, n_0 the density of the neutral gas and $\sigma(E)$ the ionization cross section as a function of the electron energy. We take for $\sigma(E)$ the same expression used in reference (1).

In Fig. 4 we show the experimental points of Cybulska and Douglas as dots with the corresponding error bars. The curves are theoretical predictions using their value of $x_0 = 0.06/4.5$ and $\alpha = 8, 10$ and 13. One observes from this figure that $\alpha = 10$, i.e., $kT = 80eV$, gives the best fit to their data.

It is important to mention that our calculation described here gives a better fit than the one previously reported in ref. (1), where we did not consider the cut off imposed on P_z as given by eq. (2.4). The improvement is better observed in the low energy part of the ion current spectrum.

3. COLLECTIVE OSCILLATIONS

One may look at the steady state of the electron cloud inside the orbitron as a gas in thermal equilibrium. Let be ρ_0 the equilibrium mass density of the electrons and p_0 the corresponding pressure. We have

$$p_0 = \rho_0 \frac{kT}{m}$$

as the equation of state of the electron gas, m is the mass of the electron.

We will now consider the deviations from these steady state values:

$$\rho(r,t) = \rho_0(r) + \rho'(r,t)$$

$$p(r,t) = p_0(r) + p'(r,t)$$

and we will show that these deviations $\rho'(r,t)$ and $p'(r,t)$ will propagate inside the cloud as pressure waves. To describe these waves we will start from the two basic equations of fluid dynamics: the equation of continuity

$$\frac{\partial \rho}{\partial t} + \vec{\nabla} (\rho \vec{v}) = 0 \qquad (3.1)$$

and Euler's equation

$$\rho \frac{\partial \vec{v}}{\partial t} = \vec{g} - \vec{\nabla} p \quad . \qquad (3.2)$$

The vector field $\vec{v}(r,t)$ is the velocity field and $\vec{g}$ is the external force density applied to the gas. From the equilibrium value we must have

$$\vec{g} = \nabla p_0$$

$$\vec{v} = 0 \quad .$$

In what follows we will derive the equation for the propagation of

$$u = p'/p_0 \quad ,$$

on the assumption that $u << 1$ and $\vec{v}$ and ρ'/ρ are of the same order as u.

We will first assume that the variation of u and p in the electron cloud are adiabatic and set

$$\frac{du}{dt} = \left(\frac{\partial u}{\partial \rho}\right)_S \frac{dp}{dt} \quad .$$

We have

$$\left(\frac{\partial \rho}{\partial p}\right)_S = \frac{m}{\gamma kT}$$

where $\gamma = 5/3$ is the ratio of the specific heat at constant pressure and at constant volume. Making use of this fact we transform the eq. (3.1) into:

$$\frac{1}{\gamma}\frac{\partial u}{\partial t} + \vec{v}.\vec{q} + \nabla.\vec{v} = 0 \qquad (3.3)$$

where

$$\vec{q} = \frac{1}{\gamma p_0} \vec{\nabla} p_0 \quad . \tag{3.4}$$

Similarly we can transform Euler's eq. (3.2) and we have

$$\frac{\partial \vec{v}}{\partial t} = - \frac{p_0}{\rho_0} \vec{\nabla} u \tag{3.5}$$

where we made use of the fact that

$$\vec{g} = \vec{\nabla} p_0$$

at equilibrium.

Eliminating $\vec{v}$ between the eqs. (3.3) and (3.5) we finally have

$$\nabla^2 u + \vec{q} . \vec{\nabla} u - \frac{1}{c^2} \frac{\partial^2 u}{\partial t} = 0 \tag{3.6}$$

where

$$c = \sqrt{\gamma p_0 / \rho_0} = \sqrt{\frac{\gamma kT}{m}}$$

is the velocity of the pressure waves in the electron gas.

For kT = 80 eV this gives

$$c = 0.0162 \; c_0$$

where c_0 is the velocity of light.

Because of the cylindrical symmetry of the orbitron $\vec{q}$, except near the end plates, is a radial vector function of r only.

To find the eigen modes of the oscillations we assume

$$u = u_r(r)u_\theta(\theta)u_z(z)\ e^{i\omega t}$$

i.e., u is separable in cylindrical coordinates. The boundary condition are

$$u_z(0) = u_z(z_0) = 0$$

$$u_\theta(0) = u_\theta(2\pi)$$

and

$$u_r(a) = u_r(b) = 0 \quad .$$

We then have

$$u_z = \sin\left(\frac{n_z \pi}{z_0} z\right)$$

$$u_\theta = \sin\left(n_\theta . \theta + \alpha\right)$$

where n_z and n_θ are integers and z_0 is the length of the orbitron.

The equation for u_r takes the form

$$\frac{d^2u_r}{dx^2} + p(x)\ \frac{du_r}{dx} + \left(\lambda - \frac{n_\theta^2}{x^2}\right)u_r = 0 \qquad (3.7)$$

with boundary conditions

$$u(x_0) = u(1) = 0$$

where x and x_0 are the dimensionless variables previously introduced,

$$p(x) = \frac{1}{\gamma \rho_0(x)} \frac{d\rho_0}{dx} + \frac{1}{x}$$

and

$$\lambda = \left(\frac{b\omega}{c}\right)^2 - \left(\frac{\pi n_z b}{z_0}\right)^2 \qquad (3.8)$$

Eq. (3.7) was solved numerically and the eigenvalues λ_{n_r, n_θ} where found where n_r is the number of nodes of the radial functions. The eigen frequencies of the oscillations are then given by

$$f_{n_r, n_\theta, n_z} = \frac{c}{2\pi b} \sqrt{\lambda_{n_r, n_\theta} + \left(\frac{\pi b n_z}{z_0}\right)^2} \quad . \qquad (3.9)$$

4. COMPARISON WITH THE EXPERIMENTAL DATA

Eq. (3.7) was solved for different values of n_θ and the eigenvalues of λ where obtained. Fixing x_0, the equation was integrated from x_0 towards $x = 1$. The values of $u_r(1)$ as a function of λ for $n_\theta = 0$ and $n_\theta = 1$ are plotted in Fig. 5. The values of λ for which $u_r(1) = 0$ are the eigenvalues looked for. Table I gives the value of λ_{n_r,n_θ} for $x_0=1/30$ and $\alpha = 8$ and 15. One observes that the value of α has an important effect over the lower values and decreases its influence for the higher values of λ_{n_r,n_θ}.

Troise (7) measured the oscillation frequencies for an orbitron with the following parameters:

$$a = 0.075\text{cm} \ , \ b = 2.25\text{cm} \ (x_0 = 1/30)$$

$$z_0 = 10.8\text{cm} \qquad V_a = 1000\text{V} \ .$$

The frequencies observed in MHz where the following:

$f_1 = 13.6 \pm 0.2$	$f_4 = 58.5 \pm 2.6$	$f_7 = 172.0 \pm 3.7$
$f_2 = 22.7 \pm 2.2$	$f_5 = 85.0 \pm 2.8$	$f_8 = 213.4 \pm 4.1$
$f_3 = 34.0 \pm 2.4$	$f_6 = 127.0 \pm 3.3$	$f_9 = 260.0 \pm 4.6$

The four high frequencies observed are identified in Table II. Let us observe that, from eq. (3.9), to obtain lower frequencies one would have to decrease c or equivalently kT, but this imples in increasing α. $\lambda_{0,0}$ increases as α increases, and

therefore one understands why it is impossible to predict a fundamental frequency below 100 MHz in Troise's orbitron. The dependence of λ_{n_r,n_θ} on α is plotted in Fig. 6.

In Table II we have adjusted the value of α (α=15) to fix the fundamental mode in 126.8 MHz. The other frequencies are therefore predictions of our theory. It is interesting to observe that these high frequencies are all identified with different θ-modes. This is justified by the further evidences given by Troise. He observed that these frequencies vary very little with z_0. He actually did not detect any significant variation with z_0, the length of orbitron. The sensitiveness of the frequencies with z_0 can easely be obteined from eq. (3.9). We have

$$\frac{f_{n_r,n_\theta,n_z}}{f_{n_r,n_\theta,n_z}} = \frac{-(\frac{\pi b n_z}{z_0})^2}{\lambda_{n_r,n_\theta} + (\frac{\pi b n_z}{z_0})^2} \cdot \frac{\Delta z_0}{z_0} \quad . \qquad (4.1)$$

If we had identified these frequencies with different values of n_z we had predicted an increase in sensitiveness to z_0 with increasing the frequency, contrary to what was observed. The way we have identified these frequencies, the larger sensitiveness is for the 127 MHz frequency and even for this one we have

$$\frac{\Delta f}{f} = (0.026)\ \frac{\Delta z_0}{z_0} \quad ,$$

what exhibits a very low sensitiveness to z_0.

Fig. 7 shows the dependence of these high frequencies on the voltage V_a of the anode, the other parameters of the orbitron being fixed. The values of the frequencies do not agree with those in Table I because Troise used a different orbitron and the parameters of this orbitron has not been reported. One observes that these frequencies are directly proportional to $\sqrt{V_a}$. It is simple to interpret this result. One expects the parameter α to be constant for a given orbitron as α, the ratio of eV_a to kT, measures the efficiency with which a given orbitron transforms the initial energy of the electrons (eV_a) into kinetic energy in the steady state. We therefore assume that kT is proportional to V_a for a given orbitron and so, c, the velocity of pressure waves in the electron cloud is proportional to $\sqrt{V_a}$ and so it is also the frequencies f_{n_r,n_θ,n_z} given by eq. (3.9). The five low frequencies repported by Troise has a different explanation as it has been put forward for the first time by Rogerio (9). His idea was that these low frequencies come from the beats of the frequencies of the normal modes of vibration. The base of his idea is the well known result of mechanics that says that non-linear terms considered as perturbations of the linear wave equation generate frequencies which are additions or subtractions of the non-perturbed frequencies. In Table III we put forward the explanation of the low frequencies as differences of normal mode frequencies calculated from our linear wave equation. We observe that the two very low frequencies come from the beat of z-modes of vibration. The third frequency (34.0 MHz) may come either from the beat of z-modes or θ-modes and the other two (58.5 and 85.0MHz) como from beats of the θ-modes as indicated in

the above mentioned Table.

In Fig. 8 we show the results of Troise for the dependence on z_0 of the low frequencies of an orbitron different from the one where the frequencies reported in Table III were measured. We observe a strong dependence on z_0, the length of the orbitron. This can be partially understood as a consequence of these frequencies be beats of normal modes of vibration. We will consider two cases corresponding to beats in the z-mode and θ-mode.

Let us consider the beat frequency $\bar{f}$ given by

$$\bar{f} = f' - f \quad .$$

From eq. (3.9) we have

$$\frac{\partial \bar{f}}{\partial z_0} = - \frac{c^2}{4 z_0^3} \left[\frac{n_z'^2}{f'} - \frac{n_z^2}{f} \right] \tag{4.2}$$

This equation shows that the sign of variation of $\bar{f}$ with z_0 depends on the fac that $\bar{f}$ comes from θ-mode ($n_z' = n_z$) or z-mode ($n_z' > n_z$). One observes then that θ-mode predicts that the frequency increases with z_0 as it has been observed by Troise. To make a quantitative comparison let us take $z_0 = 3.5$cm, as can be seen from Fig. 8. The repported V_a was 600V and we assume the other geometrical dimensions to be the same, that is a=0.075 and b=2.25. We also assume $\alpha = 15$. Under these considerations the beat between the two modes (0, 1, 1) and (0, 0, 1) gives the frequency $\bar{f} = 11.8$MHz in the region observed by Troise. From eq. (4.2) we have

$$\frac{\Delta\bar{f}}{\bar{f}} = \frac{c^2}{4z_0^2 ff'} \left(\frac{\Delta z_0}{z_0}\right)$$

and we obtain,

$$\frac{c^2}{4z_0^2 ff'} = 0.31 \quad .$$

From Fig. 8 we should have a value 10 times larger than this one. We now observe that the sensitiveness of $\bar{f}$ is proportional to z_0^{-2} and so very sensitive to the value of z_0 used. The end plates has the effect of reppelling the electron cloud and so shorten the effective length of the orbitron. As Troise's orbitrons is already very short (smaller than its diameter) we are not surprise at the disagreement of the sensitiveness of $\bar{f}$ to z_0. If we say that the end plates decreases z_0 of 2.5cm, we would get the value for $(\Delta\bar{f}/\bar{f})/(\Delta z_0/z_0)$ observed in Fig. 8.

5. CONCLUSION

We may conclude by saying that most of the experimental information of Cybulska and Douglas (2) and Troise (7) has been theoretically explained on the basis that the electron cloud inside the orbitron reaches a steady state characterized by an equilibrium temperature. The oscillations observed by Troise has been explained as pressure waves in the electron cloud. It is interesting to observe that due to the lack of a theoretical background at the time Troise took the measurements of these oscillations, his data has not been extensively recorded to give a deep insight on the behavior of the electron cloud. Nevertheless we are able to sustain that the steady state thermal equilibrium of the electrons gives a good understanding of the behavior of orbitrons.

It is interesting also to observe that orbitrons can maintain an electron cloud at temperatures of the order of 10^6 ^oK in the absence of magnetic fields and any positive charge to neutralize the electrostatic repulsion among the electrons. The cloud of electrons make a good laboratory device for studying atomic and molecular behavior under such extreme condition with the temperature controlled by the anode voltage as, by varying the anode voltage, we vary directly the temperature of the cloud but not its spatial distribution.

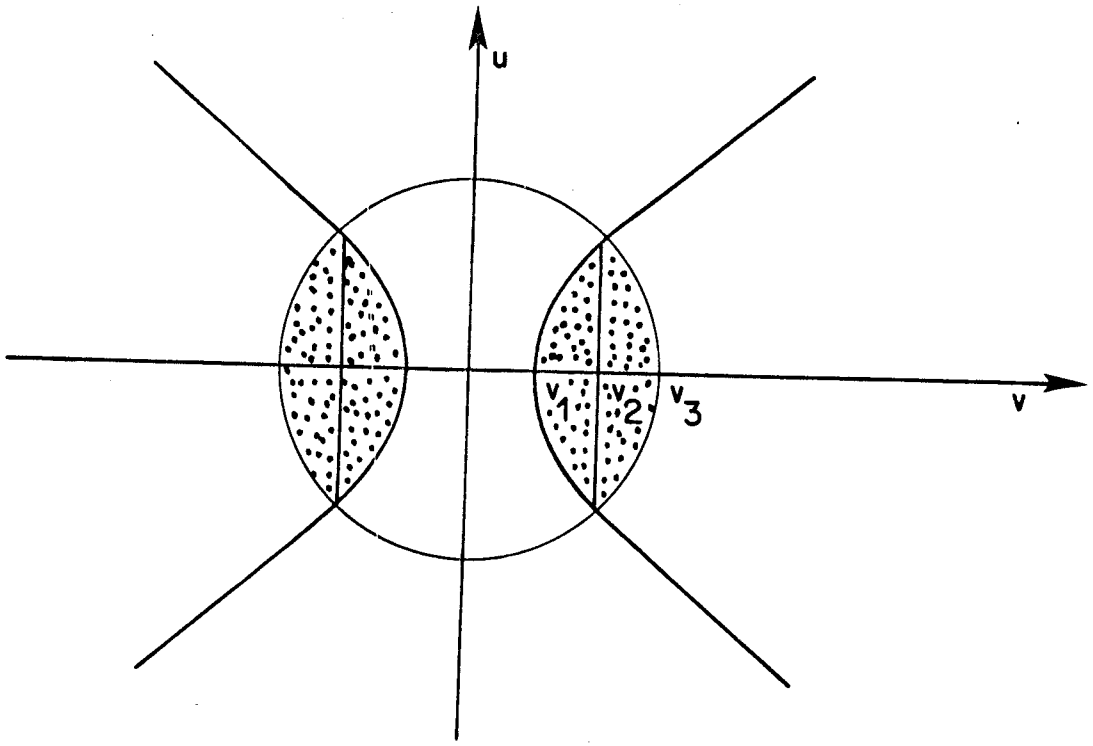

Figure 1

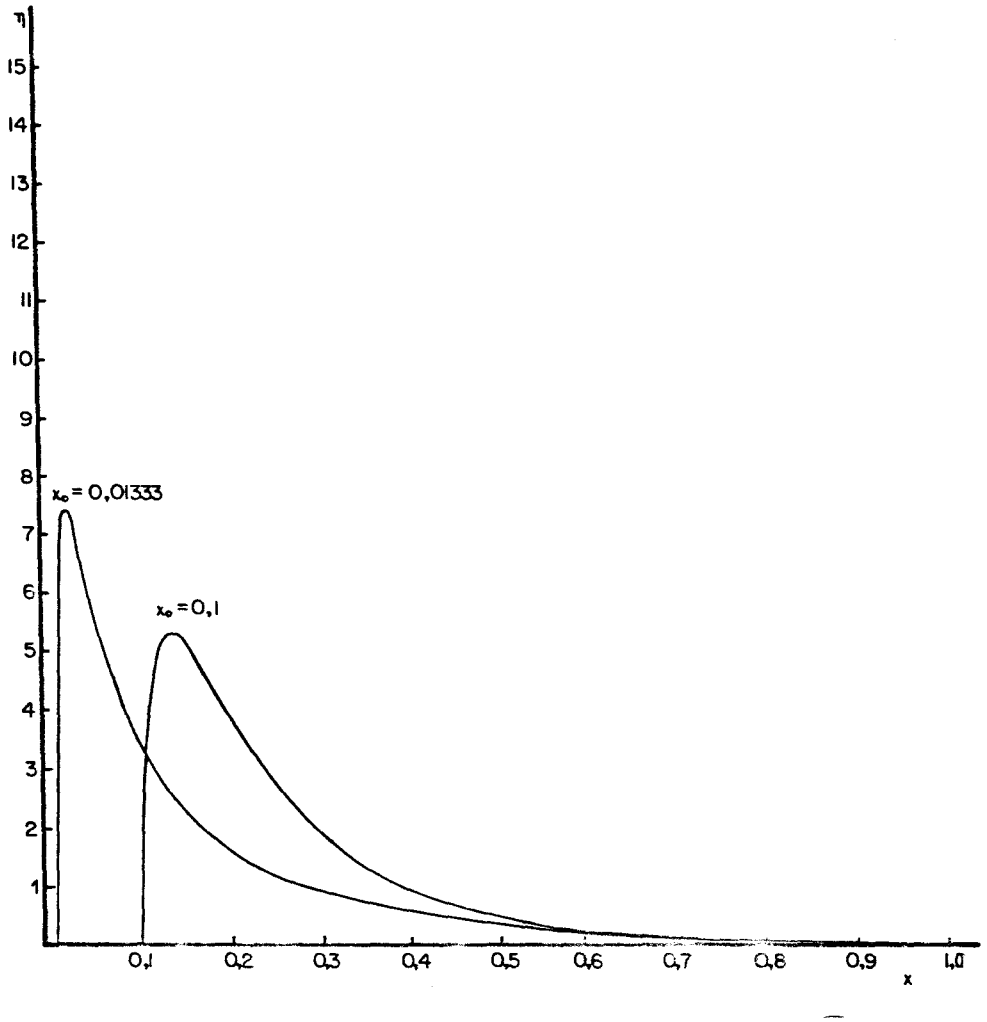
η
15
14
13
12
11
10
9
8
7
6
5
4
3
2
1
$x_0 = 0,01333$
$x_0 = 0,1$
0,1
0,2
0,3
0,4
0,5
0,6
0,7
0,8
0,9
1,0
x

Figure 2

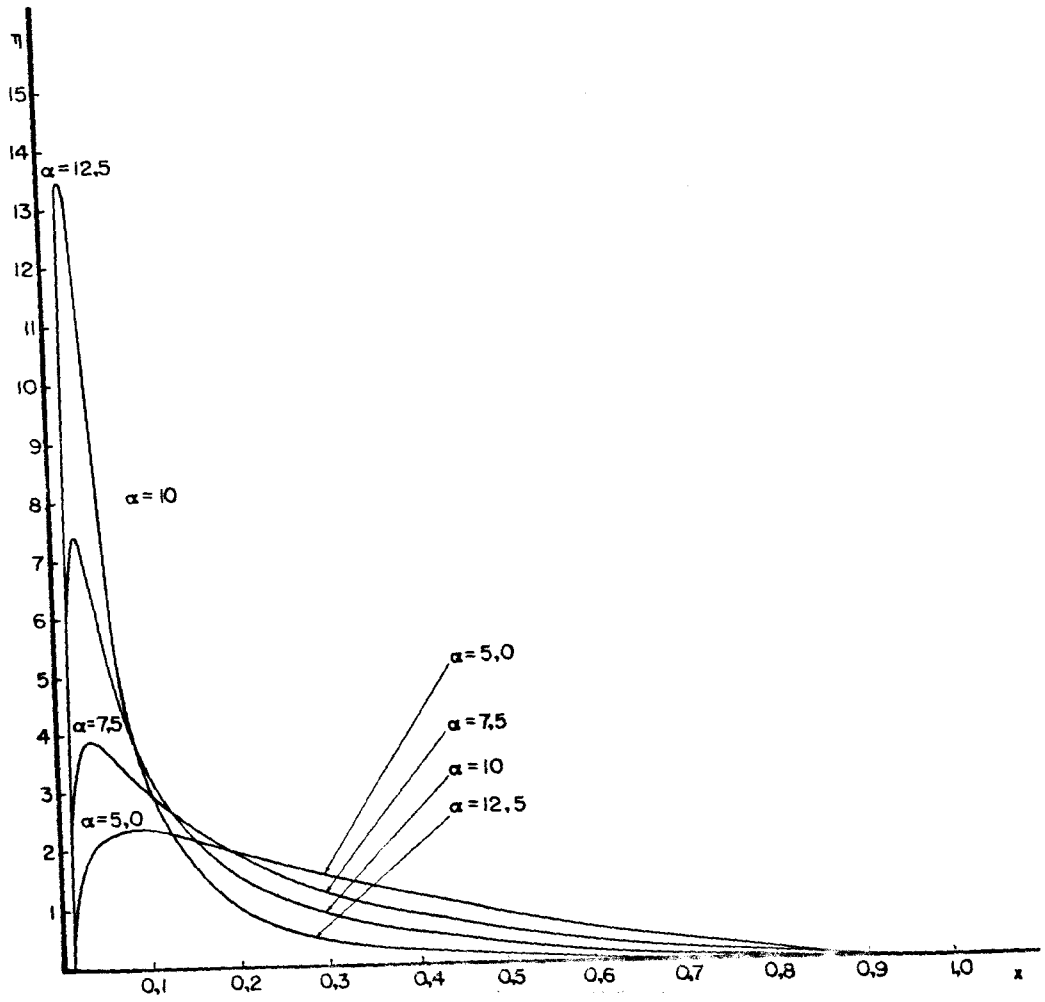
η
15
14
13
12
11
10
9
8
7
6
5
4
3
2
1
α=12,5
α=10
α=7,5
α=5,0
α=5,0
α=7,5
α=10
α=12,5
0,1
0,2
0,3
0,4
0,5
0,6
0,7
0,8
0,9
1,0
x

Figure 3

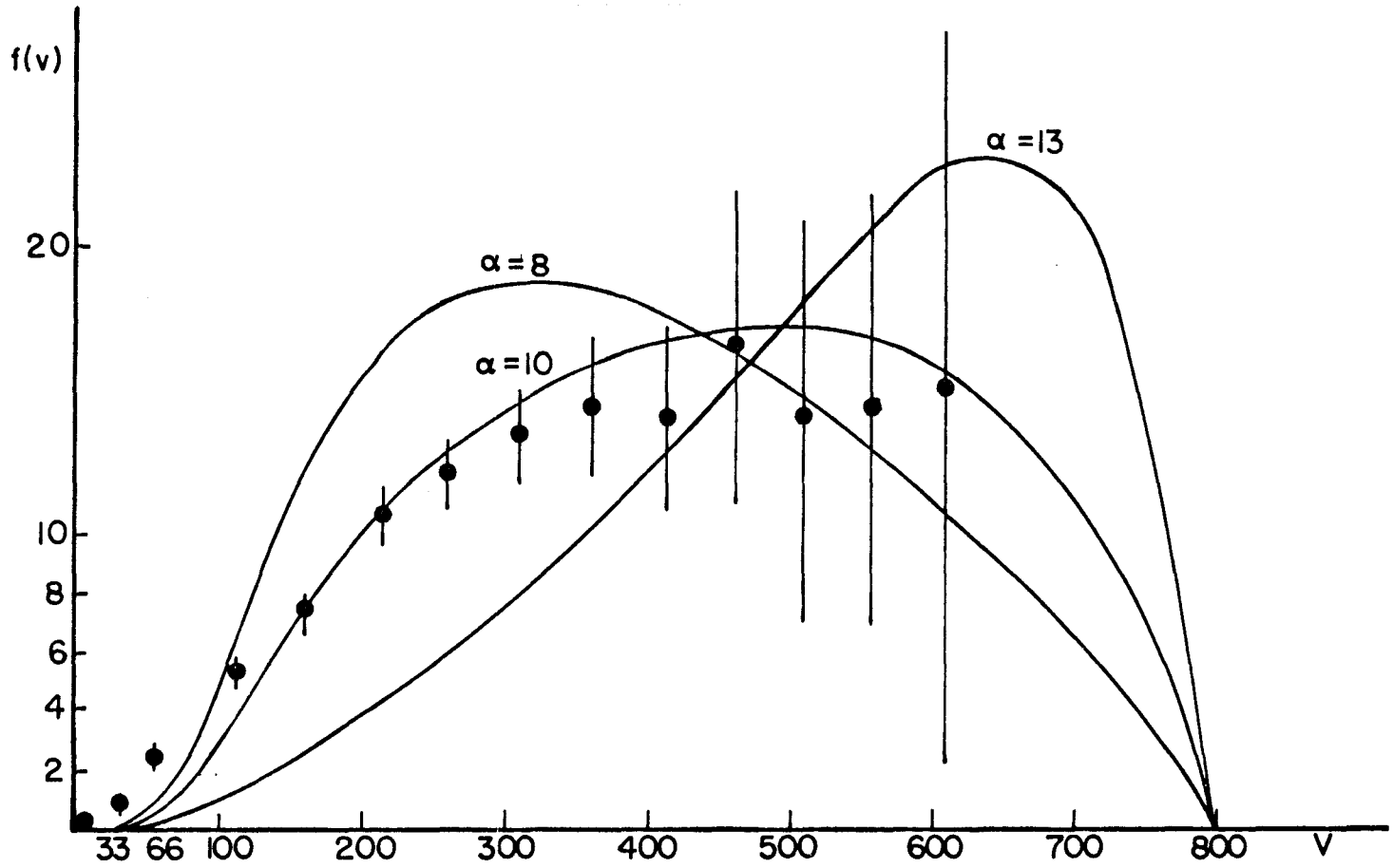

Figure 4

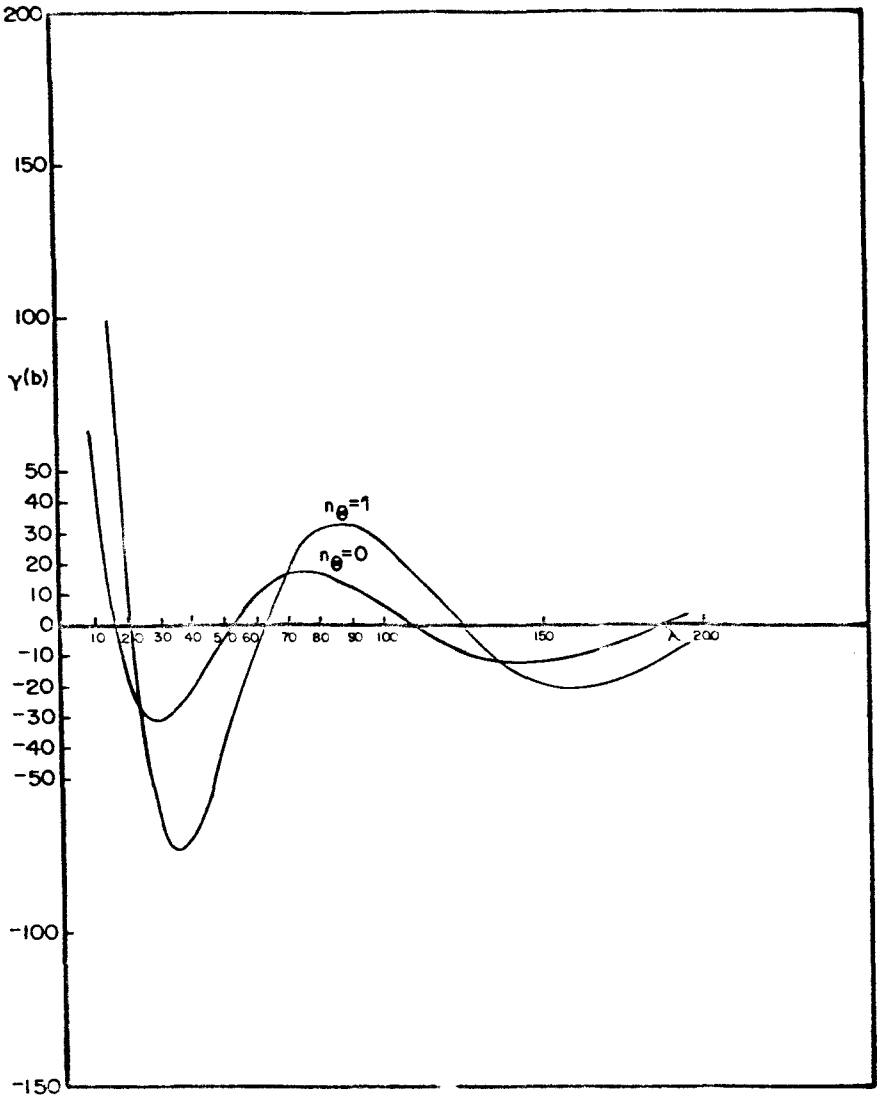
200
150
100
γ(b)
50
40
30
20
10
0
-10
-20
-30
-40
-50
-100
-150
10
20
30
40
50
60
70
80
90
100
150
λ
200
n_θ=1
n_θ=0

Figure 5

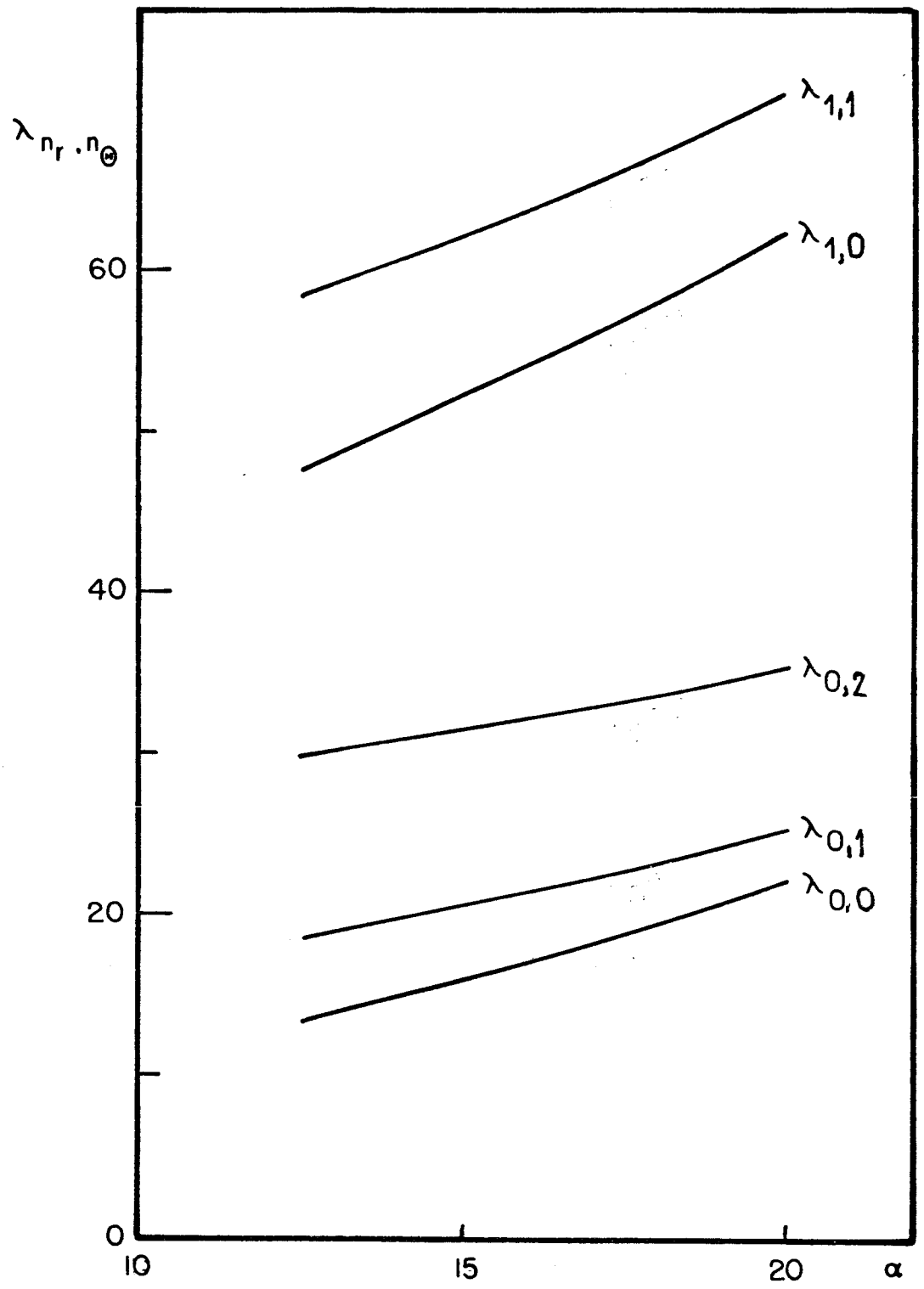
$\lambda_{n_r . n_\Theta}$
60
40
20
0
10
15
20
α
$\lambda_{1,1}$
$\lambda_{1,0}$
$\lambda_{0,2}$
$\lambda_{0,1}$
$\lambda_{0,0}$

Figure 6

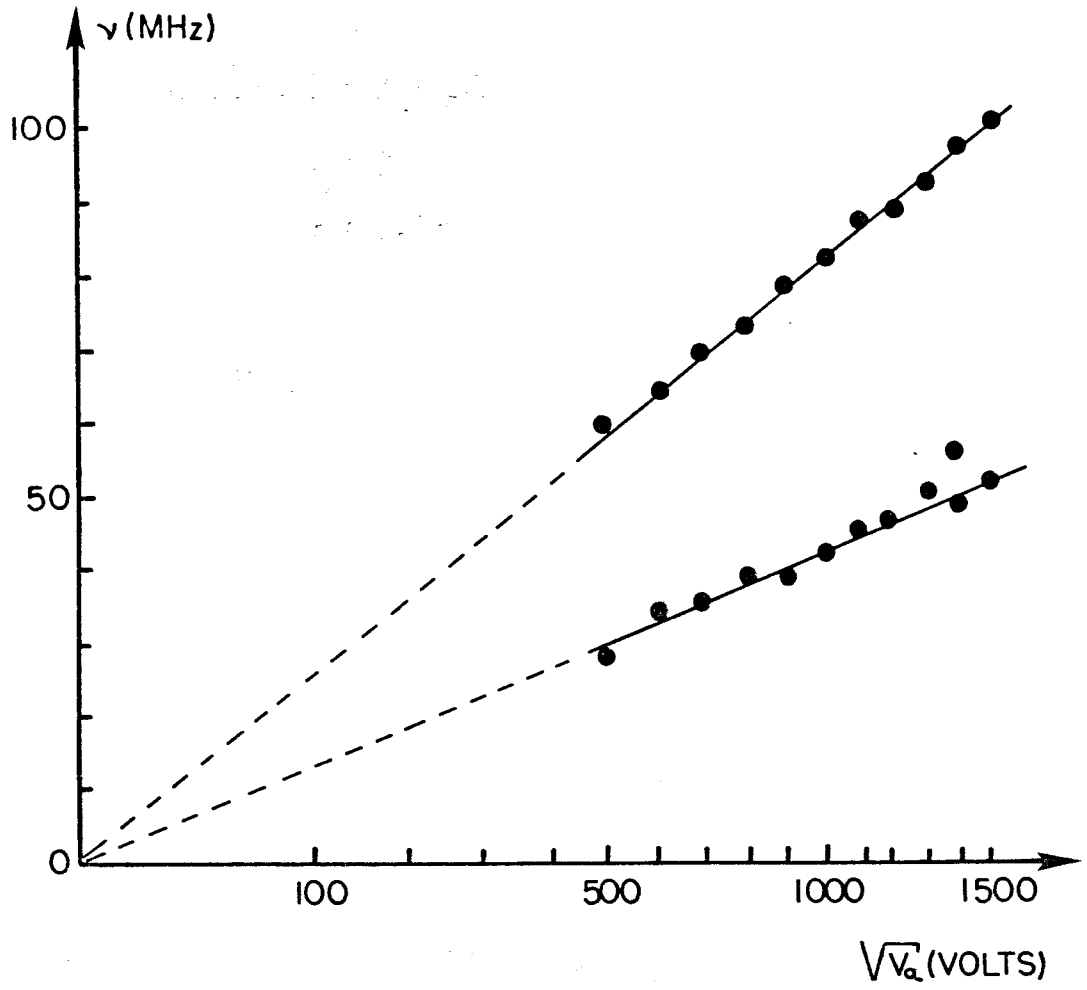

Figure 7

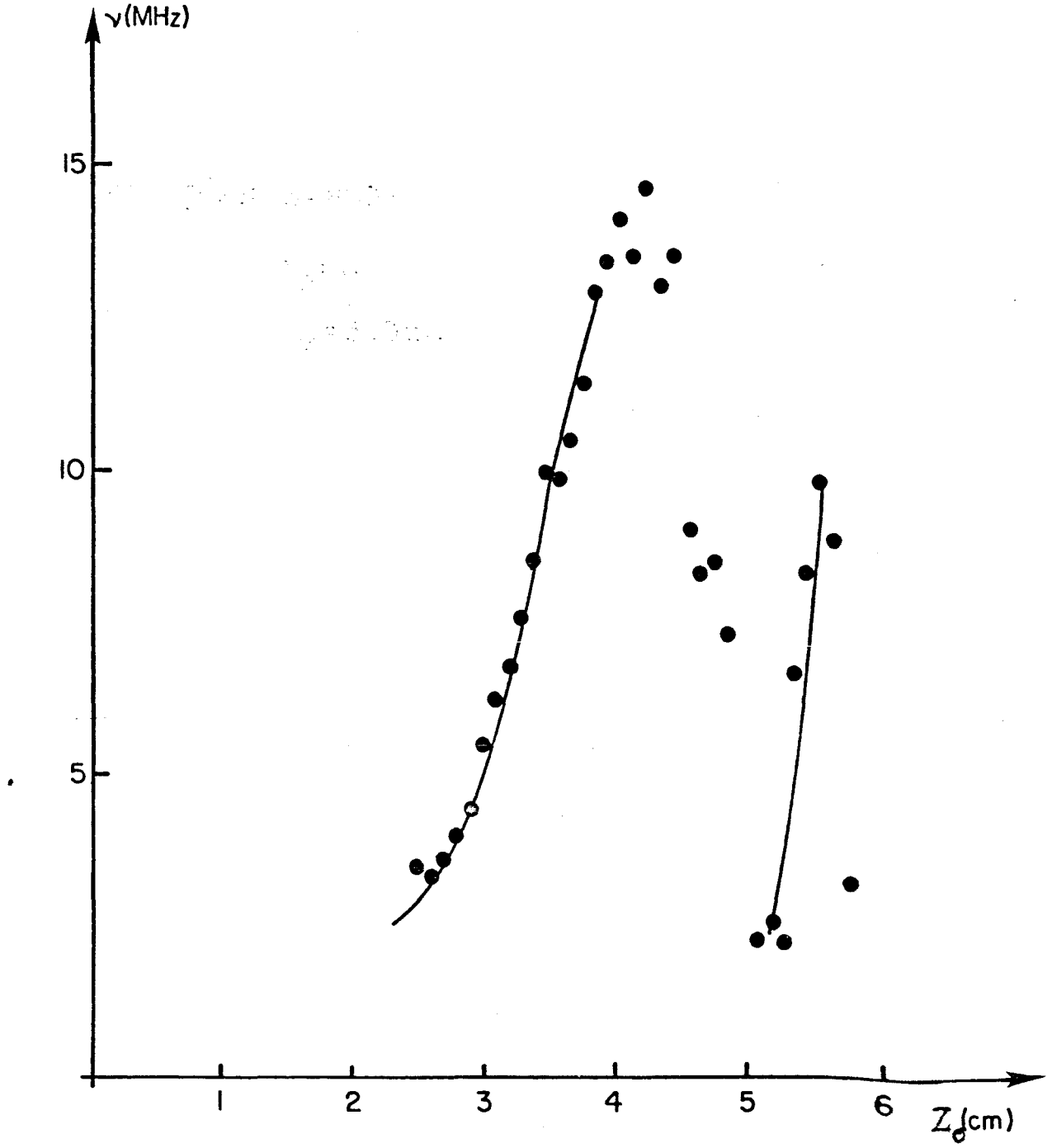

Figure 8

TABLE I

		λ_{n_r, n_θ}	
n_r	n_θ	$\alpha = 8$	$\alpha = 15$
0	0	9.3	16.0
0	1	15.3	20.6
0	2	27.0	31.4
0	3	41.9	45.8
0	4	59.7	63.2
1	0	41.1	52.1
1	1	53.0	62.0
1	2	75.6	82.4
1	3	101.6	107.3
1	4	130.7	135.8

TABLE II

Frequencies in MHz		
Experimental	Theoretical	mode (u_r, u_θ, n_z)
127 ± 3.3	126.8	(0, 0, 1)
——	143.5	(0, 1, 1)
172 ± 3.7	176.5	(0, 2, 1)
213 ± 4.1	212.8	(0, 3, 1)
260.0±4.6	249.6	(0, 4, 1)

TABLE III

Frequencies in MHz		Beat
Exp.	Theor.	$(n_r, n_\theta, n_z) - (n_r, n_\theta, n_z)$
13.6 ± 0.2	12.6	(0, 0, 3) - (0, 0, 1)
22.7 ± 2.2	22.8	(0, 0, 4) - (0, 0, 1)
	22.3	(0, 0, 5) - (0, 0, 3)
34.0 ± 2.4	33.0	(0, 2, 1) - (0, 1, 1)
	34.9	(0, 0, 5) - (0, 0, 1)
58.5 ± 2.6	58.0	(1, 2, 1) - (1, 0, 1)
85.0 ± 2.8	86.0	(0, 3, 1) - (0, 0, 1)

TABLE CAPTIONS

Table I The eigenvalues of λ_{n_r,n_θ} of eq. (3.7) for two different values of α as indicated.

Table II The theoretical identification of the modes of the high frequencies observed by Troise (7). The first collumn is the experimental values, the second collumn the theoretical value and the third collumn is the mode of the vibration. We assume the following parameters $\alpha = 15$, $a = 0.75$cm, $b = 2.25$cm, $z_0 = 10.8$ cm and $V_a = 1000$V.

Table III The theoretical identifications of the beat mode of the low frequencies observed by Troise (7). The first collumn is the experimental values, the second collumn the theoretical prediction for the frequencies both in MHz. The third collumn is the corresponding beat mode.

FIGURE CAPTIONS

Fig. 1 The traces of the two boundaries of the domain defined by eqs. (2.8) and (2.9) in the plane t=0. The coordinates v_1, v_2 and v_3 are given by eqs. (2.10), (2.11) and (2.12).

Fig. 2 The density distribution given by eq. (2.13) plotted for different values of α (eq. (2.5)) as indicated.

Fig. 3 The same as in Fig. 2 plotted for two values of x_0=0.01333 and 0.1 and α as indicated.

Fig. 4 The experimental points of Cybulska and Douglas plotted as dotts with the corresponding error bars. The curves are theoretical predictions for different values of α as indicated. The abcissa is the voltage measured to stop the ion after passing the cathode. The ordinate is the ion current.

Fig. 5 The function u_r (x = 1) as a function of λ for two values of n_θ as indicated. The zeros of $u_r(1)$ are the eigenvalues of λ_{n_r,n_θ}. $u_r(x)$ satisfies eq. (3.7) and the equilibrium density was calculated with $\alpha = 1.5$, $x_0 = 0.033$.

Fig. 6 The values of λ_{n_r,n_θ} plotted as a function of α for the values of n_r and n_θ as indicated.

Fig. 7 The dependence of two high frequencies on the anode voltage V_a. The abcissa is the $\sqrt{V_a}$. The numbers indicated are the values of V_a. The ordinate is the frequency in MHz. The data were taken from Troise (7).

Fig. 8 The dependence of low frequencies on z_0. The experimental points and the curves plotted were taken from Troise (7). The abcissa is the length z_0 of the orbitron and the ordinate is the frequency in MHz. The repported anode voltage for this set of data was 600 V.

REFERENCES

(1) M. Porto Pato and L.C. Gomes, Rev. Bras. Fis. 6 (1976) 245.

(2) E.W. Cybulska and R.A. Douglas, Vacuum 26 (1976)531.

(3) R.H. Hooverman, J. Appl. Phys. 34 (1963) 3505.

(4) F. Feaks, F.C. Muly and F.J. Brock, Nasa Publication under contract NAS-W-1137.

(5) P.R. Deichelbohrer, J. Vac. Sci., Technol.,10 (1973) 875.

(6) M. Porto Pato, Thesis, Instituto de Física, Universidade de São Paulo (1978).

(7) J.J. Troise, Thesis, Instituto de Física, Universidade de São Paulo (1970).

(8) R.A. Douglas, P. Zabrikski and R.G. Herb, Rev. Sci. Instr. 36 (1965) 1.

(9) R.F. Rogerio, Thesis, Depto. Física UnB, Brasilia, DF, Brasil (1971).